Frequency shift imaging of quantum dots with single-electron resolution

J. Zhu, M. Brink, and P. L. McEuen[a)]
Laboratory of Atomic and Solid State Physics, Department of Physics, Cornell University, Ithaca, New York 14853

(Received 25 September 2005; accepted 31 October 2005; published online 5 December 2005)

We employ atomic force microscope-based frequency shift microscopy to study the electronic properties of quantum dots formed in carbon nanotubes. The nontransport detection scheme of frequency shift allows us to probe nearly isolated quantum dots in a few electron regime. At 4 K, we observe Coulomb oscillations of quantum dots with single-electron resolution and extract the charging energy of a quantum dot. © *2005 American Institute of Physics*.
[DOI: 10.1063/1.2139623]

In recent years, a family of scanned probes based on the atomic force microscope (AFM) have been developed to investigate the electronic properties of nanostructures.[1–7] Among them, the most powerful technique is frequency shift microscopy (FSM), where the resonant frequency shift of the AFM cantilever probes the spatial gradient of the external force. Since its invention,[8] it has become the primary technique for noncontact AFM and has been used to probe quantum dots,[5–7] insulating surfaces,[9] and nanostructures.[10] Atomic resolution has been demonstrated on silicon.[11]

In this letter, we demonstrate the application of FSM to quantum dots formed on carbon nanotubes (CNTs). We obtain images of quantum dots with single electron resolution and establish a quantitative analysis to extract the charging energy. Taking advantage of the nontransport detection method of FSM, we are able to study nearly isolated quantum dots with only a few electrons or holes.

CNTs are grown on a 200 nm SiO_2/Si n^{++} wafer from patterned Fe particle clusters using chemical vapor deposition.[12] Grown CNTs are located by AFM imaging and subsequently contacted with palladium electrodes using electron-beam lithography. The carrier density of the CNT is tuned through the field effect of the Si backgate.

Our measurements were performed using a home-built ^{3}He AFM.[13] All data shown in this letter were taken at 4 K. We coat the tip of the cantilever with 25 nm of titanium to enable electrostatic force sensing and to use it as a local gate. A piezoresistive cantilever (Park Scientific Instruments) translates deflection amplitude δz into a resistance change δR, which is converted into a δV through a cryogenic Wheatstone bridge and measured with a lock-in amplifier. In addition to deflection, the resonant frequency of the cantilever shifts if the external force has a spatial gradient in the oscillating direction of the cantilever:

$$\frac{\delta f}{f_0} = -\frac{1}{2k}\frac{dF_{\text{ext}}}{dz}, \tag{1}$$

where $\delta f = f - f_0$. Equation (1) forms the basis of FSM. A schematic drawing of our setup is shown in Fig. 1. A typical cantilever used in our experiments has an intrinsic resonant frequency $f_0 = 40\,092$ Hz, a spring constant $k = 1.7$ N/m, and a high quality factor $Q = 25\,000$ at 4 K.[14] We use a phase locked loop (PLL) to track the resonant frequency of the cantilever and measure the changing frequency with a frequency counter.[15] We scan the AFM tip to obtain spatial images and measure addition spectra of quantum dots by varying voltages applied to the AFM tip, V_{tip}, and the Si backgate, V_g.

The total external force exerted on the cantilever is a sum of forces from several sources: The electrodes, the Si backgate, and the CNT under study. The force between the AFM cantilever and the CNT reads:

$$F_{\text{tube-tip}} = \frac{1}{2}\frac{dC_{\text{tube-tip}}}{dz}\Delta V_{\text{tube-tip}}^2, \tag{2}$$

where $\Delta V_{\text{tube-tip}} = V_{\text{tube}} - V_{\text{tip}} + \Phi_{\text{tube-tip}}$ is the potential difference between the CNT and the AFM tip, including the work function difference between the two objects $\Phi_{\text{tube-tip}}$.[16] $C_{\text{tube-tip}}$ is the capacitance between the tip and the CNT. The force from the Si backgate and the electrodes takes a similar functional form.

The frequency shift effect of the cantilever comes from $dF_{\text{tube-tip}}/dz$:

$$\frac{dF_{\text{tube-tip}}}{dz} = \frac{1}{2}\frac{d^2C_{\text{tube-tip}}}{dz^2}\Delta V_{\text{tube-tip}}^2 + \frac{dC_{\text{tube-tip}}}{dz}\frac{dV_{\text{tube}}}{dz}\Delta V_{\text{tube-tip}}. \tag{3}$$

The first term in Eq. (3) and similar terms from the Si backgate and electrodes are the ones relevant for standard FS imaging and give rise to images of CNT devices such as the one shown in Fig. 2(a). The CNT lies horizontally in the

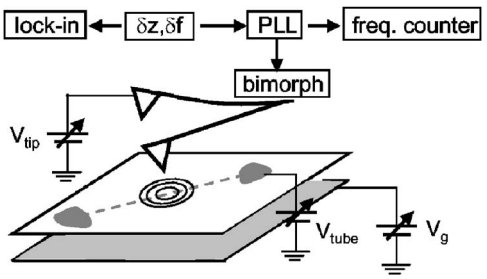

FIG. 1. FSM setup. The cantilever is always driven on resonance using a PLL controlled bimorph. We measure δz and δf of the cantilever through a lock-in amplifier and a frequency counter, respectively. The CNT is locally gated by the AFM tip or globally gated by the Si backgate. For technical convenience, we sometimes bias the electrodes as well.

[a)]Electronic mail: mceuen@ccmr.cornell.edu

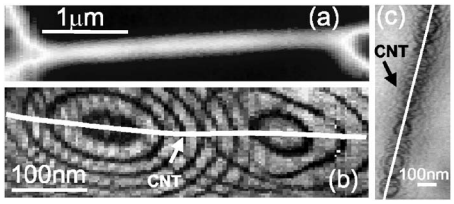

FIG. 2. Frequency shift imaging of quantum dots formed on CNTs. (a) A CNT with two electrodes. $V_{tip}=0$ V, $V_g=-3$ V, tip height $z=150$ nm. (b) Coulomb oscillations of two neighboring quantum dots formed on a CNT. $V_{tip}=-1$ V, $V_g=2.6$ V, tip height $z=100$ nm. Each contour represents the addition of one electron onto the enclosed dot. Location of CNT indicated by a white line. (c) FS detection of charge hopping among quantum dots formed on an isolated CNT. $V_{tip}=0$ V, $V_g=-1.1$ V, tip height $z=83$ nm.

middle of the figure with both electrodes partially visible on the two sides. Because of the finite size of the AFM tip and the long range characteristics of the Coulomb force, the CNT appears to be a few hundred nm wide whereas its actual diameter is only 1.3 nm.

With higher spatial resolution and lower tip height, frequency shift (FS) images of CNTs reveal additional ring structure superimposed on the CNT. Figure 2(b) shows a section of a CNT with two sets of concentric rings. The location of the CNT is indicated by a white line in the figure. It is clear that the rings are centered at specific locations on the CNT.

These rings are the Coulomb oscillations of quantum dots formed on the CNT due to local potential barriers[2–5] and are described by the second term in Eq. (3). To see this quantitatively, we substitute "dot" for "tube" in Eq. (3) and note that $dV_{dot}/dz=dV_{dot}/dq_c\cdot\partial q_c/\partial z$, where $q_c=\Delta V_{dot\text{-}tip}C_{dot\text{-}tip}+\Delta V_{dot\text{-}bg}C_{dot\text{-}bg}$ is called the control charge of the quantum dot. Since $\partial q_c/\partial z=dC_{dot\text{-}tip}/dz\Delta V_{dot\text{-}tip}$,[17] the FS due to the quantum dot term in Eq. (3) can be rewritten as:

$$\frac{\delta f^{dot}}{f_0}=-\frac{1}{2k}\frac{dF_{dot\text{-}tip}}{dz}=-\frac{1}{2k}\frac{dV_{dot}}{dq_c}\left(\frac{\partial q_c}{\partial z}\right)^2. \quad (4)$$

The charge q_c represents the desired charge on the dot according to classical electrostatics and is a smooth function of spatial and voltage variables. However, because of the large charging energy U of the dot ($U\gg k_BT$), charges hop onto the dot in discrete steps. Correspondingly, V_{dot} jumps abruptly by U/e each time a charge hops on, resulting in periodic spikes in dV_{dot}/dq_c. This periodic structure, termed Coulomb oscillations, directly enters our FS measurements as described in Eq. (4). In a V_g-swept addition spectrum as shown in Fig. 3(a), it appears as a sequence of dips, where each dip represents the addition of one charge onto the dot. In a two-dimensional spatial scan, where the AFM tip acts as a local gate, dV_{dot}/dq_c appears as a set of dark concentric rings centered on the dot. In Fig. 2(b), the two sets of rings are the Coulomb oscillations of the two neighboring quantum dots.

Using FSM, we routinely image Coulomb oscillations of quantum dots with single electron resolution. Compared to force microscopy, which was previously used for single electron imaging in Ref. 5, FSM is faster and free of the complication of dissipation.

Unlike a transport measurement, FSM poses a far less stringent requirement on the conductance level of the device. The minimum current flow through a quantum dot during a

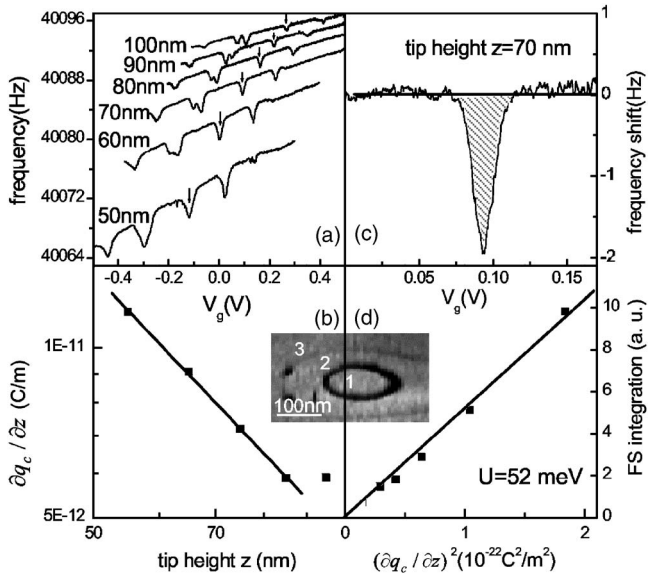

FIG. 3. Charging energy U of a quantum dot. (a) V_g dependent charge addition spectra of the quantum dot. AFM tip is centered above the dot at different heights as indicated in the figure. $V_{tip}=1$ V. The arrows mark the addition of the second hole to this dot. (b) $\partial q_c/\partial z$ as a function of the tip height z. (c) Integration of the FS signal through the Coulomb oscillation. Background is subtracted before the integration. The width of the dip (full width at half maximum=0.1 e) is mainly due to the motion of the AFM tip (1 nm). (d) FS area vs $(\partial q_c/\partial z)^2$ at different tip heights. The slope of the graph yields an average $U=52$ meV. Inset: Image of this dot with hole occupancy number. $V_g=0.3$ V, $V_{tip}=1$ V, $z=80$ nm.

charging process is of order $ef_0\sim 10$ fA, whereas a typical transport measurement requires a minimum level of pA. This advantage of FSM allows us to probe low conductance systems inaccessible to transport. In the regime where Fig. 2(b) is taken, the CNT shows no measurable conduction. Another example is given in Fig. 3, where we study a p-type quantum dot down to the very last few holes [inset of Fig. 3].

Moreover, FSM can even be applied to completely isolated systems. In Fig. 2(c), we show a FS image of an unwired CNT. Although the total number of charges on the CNT is fixed, many Coulomb oscillations are clearly visible. These oscillations are due to charge hopping among neighboring quantum dots induced by the local gating effect of the AFM tip. This example opens up the possibility of using FSM as a new charge read-out mechanism for isolated systems with internal structures, such as a double quantum dot system used in quantum computation.

In the remainder of the letter, we provide an experimental procedure to extract the charging energy of a single quantum dot.

By integrating both sides of Eq. (4), we see that the charging energy U is related to the ratio of $\int\delta f^{dot}dq_c$ and $(\partial q_c/\partial z)^2$ through k and f_0:

$$U=-\frac{\int\delta f^{dot}dq_c}{\left(\frac{\partial q_c}{\partial z}\right)^2}\cdot\frac{2ke}{f_0}. \quad (5)$$

We use the second charging dip of the dot in Fig. 3 [$q_c=1.5e$, marked by arrows in Fig. 3(a)] to illustrate the procedure. First, we determine $\partial q_c/\partial z$ by measuring the V_g-dependent addition spectrum of the dot at different tip height z and tracking V_g at the second charging dip as z changes. It follows from $\Delta q_c=0$ that

$$\frac{\partial q_c}{\partial z} = -C_{\text{dot-bg}} \frac{\Delta V_g}{\Delta z}, \tag{6}$$

where $\Delta z = 10$ nm is the height interval and ΔV_g is the shift in V_g between successive traces. The backgate capacitance $C_{\text{dot-bg}} = 1.0$ aF is calculated from the average spacing in V_g between adjacent dips on the same trace and is found to be height independent. The values of $\partial q_c / \partial z$ at different heights are plotted in Fig. 3(b). Shifts in V_g for other charging dips produce similar values.

Next, we obtain $\int \delta f^{\text{dot}} dq_c$. This integrand represents the total area of FS signal through a full Coulomb oscillation. Since we sweep V_g in our experiment, $dq_c = C_{\text{dot-bg}}\ \mathrm{d}V_g$. An illustration of the integration is given in Fig. 3(c) for $z = 70$ nm.

To extract U, we plot in Fig. 3(d) $\int \delta f^{\text{dot}} dq_c$ versus $(dq_c/dz)^2$ obtained at different heights. The slope of the linear fit yields an average $U = 52$ meV, which corresponds to a total capacitance of $\mathrm{C}_{\text{tot}} = e^2/U = 3.0$ aF.

To obtain U, it is sufficient to measure $\int \delta f^{\text{dot}} dq_c$ and $(dq_c/dz)^2$ at one specific height. The evident linear relationship between the two quantities in Fig. 3(d) indicates a height-independent U. This convergence gives us additional confidence in the applicability of Eq. (5).

The above procedure demonstrates how the charging energy of a quantum dot can be extracted quantitatively from FS measurements. We emphasize that the p-dot exists in the nonconducting regime of the CNT, inaccessible to transport approach. This measurement highlights the strength of the FS technique, i.e., its applicability to nearly isolated systems.

In conclusion, we have employed FSM to study one-dimensional quantum dots formed on CNTs. In addition to achieving single electron resolution, we are able to quantitatively extract the charging energy of a quantum dot from FS measurements. The nontransport detection scheme of FSM makes it a promising tool for studying single terminal or isolated systems that are inaccessible to transport methods.

The authors thank Michael Woodside for discussions. This work is supported by the NSF through the Center for Nanoscale Systems and by NASA through the Institute for Nanoelectronics and Computing.

[1] M. A. Topinka, B. J. LeRoy, S. E. J. Shaw, E. J. Heller, R. M. Westervelt, K. D. Maranowski, and A. C. Gossard, Science **289**, 2323 (2000).
[2] S. J. Tans and C. Dekker, Nature (London) **404**, 834 (2000).
[3] A. Bachtold, M. S. Fuhrer, S. Plyasunov, M. Forero, E. H. Anderson, A. Zettl, and P. L. McEuen, Phys. Rev. Lett. **84**, 6082 (2000).
[4] M. Bockrath, W. J. Liang, D. Bozovic, J. H. Hafner, C. M. Lieber, M. Tinkham, and H. Park, Science **291**, 283 (2001).
[5] M. T. Woodside and P. L. McEuen, Science **296**, 1098 (2002).
[6] A. Pioda, S. Kicin, T. Ihn, M. Sigrist, A. Fuhrer, K. Ensslin, A. Weichselbaum, S. E. Ulloa, M. Reinwald, and W. Wegscheider, Phys. Rev. Lett. **93**, 216801 (2004).
[7] R. Stomp, Y. Miyahara, S. Schaer, Q. Sun, H. Guo, and P. Grutter, Phys. Rev. Lett. **94**, 056802 (2005).
[8] T. R. Albrecht, P. Grutter, D. Horne, and D. Rugar, J. Appl. Phys. **69**, 668 (1991).
[9] E. Bussmann, D. J. Kim, and C. C. Williams, Appl. Phys. Lett. **85**, 2538 (2004).
[10] K. R. Brown, L. Sun, and B. E. Kane, Rev. Sci. Instrum. **75**, 2029 (2004).
[11] F. J. Giessibl, Appl. Phys. Lett. **76**, 1470 (2000).
[12] J. Kong, H. T. Soh, A. M. Cassell, C. F. Quate, and H. J. Dai, Nature (London) **395**, 878 (1998).
[13] K. McCormick, Ph.D. thesis, U. C. Berkeley (1998).
[14] We determine the spring constant of the cantilever by measuring its thermal motion at 77 K.
[15] A typical setup has a frequency resolution of 0.02 Hz/$\sqrt{\text{Hz}}$. This leads to a charge sensitivity of $1.0 \times 10^{-3}\ e/\sqrt{\text{Hz}}$ on the Coulomb oscillation shown in Fig. 3(c).
[16] A typical value of $\Phi_{\text{tube-tip}}$ is -0.13 V.
[17] In a more general situation where $dC_{\text{dot-bg}}/dz \neq 0$, Eq. (4) remains valid. This can be proven by inserting in Eq. (2) an additional force term $\frac{1}{2} dC_{\text{dot-bg}}/dz \Delta V_{\text{dot-bg}}^2$ and repeat the derivation for δf^{dot}.